

e^+e^- production in pA reactions at SIS energies *

E. L. Bratkovskaya

Institut für Theoretische Physik, Universität Giessen

35392 Giessen, Germany

Abstract

Detailed predictions for dilepton production from pA reactions at SIS energies are presented within a semi-classical BUU transport model that includes the off-shell propagation of vector mesons nonperturbatively and calculates the width of the vector mesons dynamically. Different scenarios of in-medium modifications of vector mesons, such as collisional broadening and dropping vector meson masses, are investigated and the possibilities for an experimental observation of in-medium effects in pA reactions at 1–4 GeV are discussed for a variety of nuclear targets.

PACS: 25.75.Dw, 13.30.Ce, 12.40.Yx, 12.40.Vv, 25.40.-h

Keywords: particle and resonance production; leptonic and semileptonic decays; hadron models; vector-meson dominance, nucleon-induced reactions

*Work supported by GSI and BMBF

I. INTRODUCTION

The modification of hadron properties in the nuclear matter are of fundamental interest (cf. Refs. [1–5]) as QCD sum rules [4–6] as well as QCD inspired effective Lagrangian models [1–3,7–13] predict significant changes of the vector mesons (ρ , ω and ϕ) with the nuclear density. A more direct evidence for the modification of vector mesons has been provided by the enhanced production of lepton pairs above known sources in nucleus-nucleus collisions at SPS energies [14–17]. As proposed by Li, Ko, and Brown [18] and Ko et al. [19], the observed enhancement in the invariant mass range $0.3 \leq M \leq 0.7$ GeV might be due to a shift of the ρ -meson mass following Brown/Rho scaling [1] or the Hatsuda and Lee sum rule prediction [4]. The microscopic transport studies in Refs. [20–24] for these systems support these results [18,19,25,26]. However, also more conventional approaches that describe a melting of the ρ -meson in-medium due to the strong hadronic coupling (along the lines of Refs. [7–10,13]) were found to be compatible with the CERES data [10,20,28].

An alternative way to provide independent information about the hadron properties in the medium is to use more elementary probes such as pions, protons or photons as incoming particles. In such reactions the nuclear matter is close to the ground state, i.e. at normal nuclear density, however, in-medium effects might be still significant to be observed experimentally.

In this paper, therefore, the study of dilepton production from heavy-ion, pion-nucleus collisions (cf. [23,27]) and photon-nucleus reactions [29] is extended to proton-nucleus reactions. Whereas earlier studies on $p + A$ reactions have involved a perturbative scheme for vector meson production and their dileptonic decay [30,31] the latter processes will be evaluated nonperturbatively on the basis of the resonance model [29,32] in this work and the collisional width will be calculated dynamically as a function of nucleon density, mass and momentum of the vector mesons. Furthermore, the off-shell propagation of the vector mesons – adopted from Refs. [42,43] – will be included consistently.

One might argue that $p + A$ reactions should yield similar dilepton spectra than π or

γ induced reactions on nuclear targets. However, it is not clear if the sensitivity to vector meson in-medium effects is the same in $\gamma + A$, $\pi + A$ or $p + A$ reactions since in $\gamma + A$ reactions the nucleus is illuminated rather uniformly while in π, p induced reactions the initial reaction happens close to the surface. Note, that the wavelength of the impinging hadron is short compared to the distance between nucleons in the target such that such classical considerations may be employed. Furthermore, in $\pi + A$ reactions initially high mass resonances are excited in the πN reaction whereas in $p + A$ reactions the excitation of high mass resonances – which have some ρ meson decay width – is suppressed since the energy is shared between two nucleons and a substantial longitudinal kinetic energy is left. Thus it is not obvious that all reactions finally result in similar dilepton spectra. On the other hand, it is of importance that all reactions (including $A + A$) are calculated within the same approach.

The analysis of dilepton production from $p + A$ reactions is of special interest with respect to the future dilepton experimental program of the HADES Collaboration at GSI. The detailed microscopic calculations on the basis of the resonance Boltzmann-Uehling-Uhlenbeck (BUU) model [29,32] will thus be performed for dilepton production in the systems to be measured experimentally, i.e. pC , pCa , pPb at proton energies of $E = 1.0, 2.0, 3.0$ and 4.0 GeV.

In these calculations different scenarios of in-medium modifications of vector mesons such as the 'dropping mass' scenario – following Brown/Rho scaling [1] – or the Hatsuda and Lee sum-rule prediction [4] as well as the effect of collisional broadening (cf. e.g. [33]) will be employed including, however, a dynamical width of the vector mesons that is calculated dynamically and consistent with the vector meson production/absorption amplitudes (or probabilities).

The paper is organized as follows: In Section 2 the underlying resonance model, that enters the coupled-channel BUU transport approach is presented. In Section 3 detailed predictions for these reactions are given employing a high mass resolution for the dilepton pair of $\Delta M = 10$ MeV in view of upcoming experiments with the HADES detector at GSI Darmstadt. Section 4 contains a summary and discussion of open problems.

II. DESCRIPTION OF THE MODEL

A. The resonance approach

The analysis of dilepton production from pC , pCa and pPb collisions is performed within the resonance approach of Refs. [29,32]. This model is based on the resonance concept of nucleon-nucleon and meson-nucleon interactions at low invariant energy \sqrt{s} [34] by adopting all resonance parameters from the Manley analysis [35]; all states with at least 2 stars in Ref. [35] are taken into account: $P_{33}(1232)$, $P_{11}(1440)$, $D_{13}(1520)$, $S_{11}(1535)$, $P_{33}(1600)$, $S_{31}(1620)$, $S_{11}(1650)$, $D_{15}(1675)$, $F_{15}(1680)$, $P_{13}(1879)$, $S_{31}(1900)$, $F_{35}(1905)$, $P_{31}(1910)$, $D_{35}(1930)$, $F_{37}(1950)$, $F_{17}(1990)$, $G_{17}(2190)$, $D_{35}(2350)$. These resonances couple to the following channels: $N\pi$, $N\eta$, $N\omega$, ΛK , $\Delta(1232)\pi$, $N\rho$, $N\sigma$, $N(1440)\pi$, $\Delta(1232)\rho$ with respect to the production and decay.

It has been shown in Ref. [34] that the resonance model provides a good description of the experimental data on one- and two-pion production in nucleon-nucleon collisions at low energy. However, with increasing bombarding energy the resonance contributions underestimate the data; the missing yield is then treated as a background term to the resonance amplitude. This background term 'mimics' t -channel particle production mechanism as well as other non-resonance contributions (e.g., direct $NN \rightarrow NN\pi$, without creating an intermediate resonance).

With increasing energy, furthermore, multiparticle production becomes more and more important. The high energy collisions – above $\sqrt{s} = 2.6$ GeV for baryon-baryon collisions and $\sqrt{s} = 2.2$ GeV for meson-baryon collisions – are described by the LUND string fragmentation model FRITIOF [36]. This aspect is similar to that used in the HSD (Hadron-String-Dynamics) approach [22,23,37] and the UrQMD model [38].

This combined resonance-string approach allows to calculate particle production in baryon-baryon and meson-baryon collisions from low to high energies. The collisional dynamics for proton-nucleus reactions, furthermore, is described by the coupled-channel BUU transport approach [29,32] that is based on the same elementary cross sections.

B. Dilepton production

The dilepton production within the resonance model can be schematically presented in the following way:

$$BB \rightarrow RX \tag{1}$$

$$mB \rightarrow RX \tag{2}$$

$$R \rightarrow e^+e^-X, \tag{3}$$

$$R \rightarrow mX, m \rightarrow e^+e^-X, \tag{4}$$

$$R \rightarrow R'X, R' \rightarrow e^+e^-X, \tag{5}$$

i.e. in a first step a resonance R might be produced in baryon-baryon (BB) or meson-baryon (mB) collisions – (1), (2). Then this resonance can couple to dileptons directly – (3) (e.g., Dalitz decay of the Δ resonance: $\Delta \rightarrow e^+e^-N$) or decays to a meson m (+ baryon) – (4) which produces dileptons via direct decays (ρ, ω) or Dalitz decays (π^0, η, ω). The resonance R might also decay into another resonance R' – (5) which later produces dileptons via Dalitz decay or again via meson decays (e.g., $D_{35}(1930) \rightarrow \Delta\rho, \Delta \rightarrow e^+e^-N, \rho \rightarrow e^+e^-$). Note, that in the combined model the final particles – which couple to dileptons – can be produced also via non-resonant mechanisms, i.e. 'background' at low and intermediate energies and string decay at high energies.

The electromagnetic part of all conventional dilepton sources – π^0, η, ω and Δ Dalitz decay, direct decay of vector mesons ρ, ω and pn bremsstrahlung – are treated in the same way as described in detail in Ref. [39]– where dilepton production in pp and pd reactions has been studied – and should not be repeated here again. A description of the elementary dilepton sources can be found also in Ref. [40].

III. IN-MEDIUM EFFECTS ON DILEPTON PRODUCTION.

A. Collisional broadening and in-medium propagation

In line with Refs. [41] the effects of collisional broadening for the vector meson width have been implemented:

$$\Gamma_V^*(M, |\vec{p}|, \rho) = \Gamma_V(M) + \Gamma_{coll}(M, |\vec{p}|, \rho), \quad (6)$$

where the collisional width is given as

$$\Gamma_{coll}(M, |\vec{p}|, \rho) = \gamma \rho \langle v \sigma_{VN}^{tot} \rangle. \quad (7)$$

Here $v = |\vec{p}|/E$, \vec{p} , E are the vector meson velocity, 3-momentum and energy with respect to the target at rest, γ is the Lorentz factor for the boost to the rest frame of the vector meson, ρ the nuclear density and σ_{VN}^{tot} is the meson-nucleon total cross section calculated within the Manley resonance model [35], while $\Gamma_V(M)$ denotes the vacuum width according to the Manley parametrization [35] (for details see Ref. [29]). In Eq. (7) the brackets stand for an average over the Fermi distribution of the nucleons.

While propagating through the nuclear medium the total width of the vector meson Γ_V^* (6) changes dynamical and its spectral function is modified according to the real part of the vector meson self energy $Re\Sigma^{ret}$, as well as by the imaginary part of the self energy ($\Gamma_V^* \simeq -Im\Sigma^{ret}/M$) following

$$A_V(M) = \frac{2}{\pi} \frac{M^2 \Gamma_V^*}{(M^2 - M_0^2 - Re\Sigma^{ret})^2 + (M\Gamma_V^*)^2}, \quad (8)$$

which is the in-medium form for a boson spectral function.

Since the vector mesons are produced at finite density in line with the mass-distribution (8) with $\Gamma_V^* \neq \Gamma_V$ in the kinematical allowed mass regime, their spectral function has to merge the vacuum spectral function when propagating out of the medium. To specify the actual (and general) problem let us consider the decay of the $N(1520)$ to a nucleon and a ρ -meson: Only a low mass 'slice' of ρ mesons can be populated due to energy conservation; such low mass ρ test-particles can only change their actual mass by collisions with other hadrons in the approach of [29]. In practice, however, such test-particles do not scatter often enough to reconstruct the vacuum spectral function when propagating out of the

nucleus. As a consequence such low mass ρ 's may propagate to the vacuum without collisions and radiate dileptons for a long time in the vacuum since their lifetime, given by the inverse 2 pion decay width, is very long in the vacuum for low invariant mass. This 'artefact' is enhanced by the dilepton radiation probability which – due to the virtual photon propagator and a phase-space factor – is $\sim M^{-3}$. As a consequence the mass differential dilepton spectrum shows a large peak close to $M = 2m_\pi$ (cf. Fig. 14 of [29]). Some 'prescriptions' have been used in [29] to cure the problem: either an 'instantaneous' ρ meson decay, a minimum 2 pion width of 10 MeV or a mass- and density-dependent real 'potential' for the ρ 's (by Monte Carlo) which reconstructs the vacuum ρ spectral function when the test-particles propagate out of the nucleus. The differences between these 'prescriptions' are dramatic for $M \leq 0.4$ GeV but become small for $M \geq 0.5$ GeV (cf. Fig. 14 of [29]).

In order to avoid the 'low-mass ambiguities' from such 'numerical prescriptions', which do not appear in perturbative calculational schemes, in this study the general off-shell equations of motion from Refs. [42,43] have been employed. Related equations for the nonrelativistic case have been given in Ref. [44]. In [42,43] the equations of motion for test particles with momentum \vec{P}_i , energy ε_i at position \vec{X}_i – representing a short-lived off-shell particle – have been extended to

$$\frac{d\vec{X}_i}{dt} = \frac{1}{2\varepsilon_i} \left[2\vec{P}_i + \vec{\nabla}_{P_i} \text{Re}\Sigma^{ret}_{(i)} + \frac{\varepsilon_i^2 - \vec{P}_i^2 - M_0^2 - \text{Re}\Sigma^{ret}_{(i)}}{\Gamma_{(i)}} \vec{\nabla}_{P_i} \Gamma_{(i)} \right], \quad (9)$$

$$\frac{d\vec{P}_i}{dt} = \frac{1}{2\varepsilon_i} \left[\vec{\nabla}_{X_i} \text{Re}\Sigma^{ret}_{(i)} + \frac{\varepsilon_i^2 - \vec{P}_i^2 - M_0^2 - \text{Re}\Sigma^{ret}_{(i)}}{\Gamma_{(i)}} \vec{\nabla}_{X_i} \Gamma_{(i)} \right], \quad (10)$$

$$\frac{d\varepsilon_i}{dt} = \frac{1}{2\varepsilon_i} \left[\frac{\partial \text{Re}\Sigma^{ret}_{(i)}}{\partial t} + \frac{\varepsilon_i^2 - \vec{P}_i^2 - M_0^2 - \text{Re}\Sigma^{ret}_{(i)}}{\Gamma_{(i)}} \frac{\partial \Gamma_{(i)}}{\partial t} \right], \quad (11)$$

where the notation $F_{(i)}$ implies that the function is taken at the coordinates of the test particle, i.e. $F_{(i)} \equiv F(t, \vec{X}_i(t), \vec{P}_i(t), \varepsilon_i(t))$. In Eqs. (9)-(11) $\text{Re}\Sigma^{ret}$ denotes the real part of the retarded self energy while $\Gamma = -1/2\text{Im}\Sigma^{ret}$ stands for the imaginary part in shorthand notation. Note, that in (9)-(11) energy derivatives of the self energy Σ^{ret} have been discarded (cf. [42,43]). This should work out well according to the model studies in [43]

for the proton-nucleus case.

Furthermore, following Ref. [42] and using $M^2 = P^2 - Re\Sigma^{ret}$ as an independent variable instead of the energy $P_0 \equiv \varepsilon$, Eq. (11) turns to

$$\frac{dM_i^2}{dt} = \frac{M_i^2 - M_0^2}{\Gamma_{(i)}} \frac{d\Gamma_{(i)}}{dt} \quad (12)$$

for the time evolution of the test-particle i in the invariant mass squared [42,43].

Apart from the propagation in the real potential $\sim Re\Sigma/2\varepsilon$ the equations (9) – (12) include the dynamical changes due to the imaginary part of the self energy $Im\Sigma^{ret} \sim -M\Gamma_V^*$ with Γ_V^* from (6). It is worth to mention that the deviation from the pole mass, i.e. $\Delta M^2 = M^2 - M_0^2$, follows the equation

$$\frac{d}{dt}\Delta M^2 = \frac{\Delta M^2}{Im\Sigma^{ret}} \frac{d}{dt}Im\Sigma^{ret}, \quad (13)$$

which expresses the fact that the off-shellness in mass is proportional to the total width Γ_V^* . Note, furthermore, that the equations of motion (9) – (12) conserve the particle energy ε if the self energy Σ^{ret} does not depend on time explicitly (cf. Refs. [42,43]), which is approximately the case for $p + A$ reactions.

In this study the effects of collisional broadening described by Γ_{coll} (7) with and without an explicit potential ($Re\Sigma^{ret}$) for the vector mesons will be considered (cf. next Subsection).

B. 'Dropping' vector meson mass

In order to explore the observable consequences of vector meson mass shifts at finite nuclear density the in-medium vector meson masses are modeled according to the Hatsuda and Lee [4] or Brown/Rho scaling [1] as

$$M^* = M_0 \left(1 - \alpha \frac{\rho(\vec{r})}{\rho_0} \right), \quad (14)$$

where $\rho(\vec{r})$ is the nuclear density at the resonance decay, $\rho_0 = 0.16 \text{ fm}^{-3}$ and $\alpha \simeq 0.18$ for the ρ and ω . The choice (14) corresponds to

$$Re\Sigma^{ret} = M_0^2 \left(\left(\alpha \frac{\rho}{\rho_0} \right)^2 - 2\alpha \frac{\rho}{\rho_0} \right) \quad (15)$$

in (9) – (12), which is dominated by the attractive linear term in ρ/ρ_0 at nuclear matter density ρ_0 .

The in-medium vector meson masses M^* (14) in principle have to be taken into account in the production part as well as for absorption reactions and for propagation. This is implemented for the low energy reactions with nucleon resonances. Note, however, that the vector mesons produced by the FRITIOF model – as implemented in the transport approach [29] – have masses according to the free spectral function. This approximation might not be severe since the vector mesons from string decay at high energy have high momenta with respect to the target nucleus where pole-mass shifts are expected to be small [13,45]. Furthermore, the $N\rho$ -width of the baryonic resonances at finite density [29] has not been modified. Such modifications are out of the scope of the present model.

IV. NUMERICAL RESULTS

A. spatial distribution of e^+e^- production from vector meson decays

As mentioned in the introduction dilepton studies from $p + A$ reactions allow to investigate the vector meson properties at moderate densities under well controlled conditions and provide complementary information to π or γ induced reactions on nuclei. To this aim the average density distribution of a Pb -nucleus at rest in the laboratory is shown in Fig. 1 (upper left part) as well as the spatial distribution in the first pN collisions (upper right part). Here the spatial distribution $\frac{1}{b} \frac{dN}{dbdz}$ is displayed in cylindrical coordinates $b = (x^2 + y^2)^{1/2}$ and z , where z is directed along the beam axis and the proton is impinging on the nucleus from the left side.

The lower part of Fig. 1 displays the spatial distribution for ρ -meson (left part) and ω -meson (right part) decays to dileptons. At low bombarding energy most of the ρ 's stem from the decay of baryonic resonances formed in primary pN and secondary πN collisions. Thus, ρ 's are produced inside the nucleus close to the surface, i.e. at normal

nuclear density. Since ρ -mesons have a short life time, they decay to dileptons basically inside the nucleus. On the contrary, the ω -mesons are formed dominantly in primary pN collisions and have a longer life time, such that the ω spatial distribution is more elongated and part of the ω 's decay outside the nucleus.

B. $p + A$ collisions from 1–4 GeV

1. Invariant mass distributions

In Fig. 2 the calculated dilepton invariant mass spectra $d\sigma/dM$ are presented for $p+C$ collisions from 1.0 – 4 GeV (including an experimental mass resolution $\Delta M = 10$ MeV) without in-medium modifications (bare masses) – left part, and applying the collisional broadening + dropping mass scenario – right part. The thin lines indicate the individual contributions from the different production channels; *i.e.* starting from low M : Dalitz decay $\pi^0 \rightarrow \gamma e^+ e^-$ (short dashed line), $\eta \rightarrow \gamma e^+ e^-$ (dotted line), $\Delta \rightarrow N e^+ e^-$ (dashed line), $\omega \rightarrow \pi^0 e^+ e^-$ (dot-dashed line), for $M \approx 0.7$ GeV: $\omega \rightarrow e^+ e^-$ (dot-dashed line), $\rho^0 \rightarrow e^+ e^-$ (short dashed line). The full solid line represents the sum of all sources considered here. The dominant contribution at low M ($> m_{\pi^0}$) is the η Dalitz decay, however, for $M > 0.4$ GeV the dileptons stem basically all from direct vector meson decays (ρ and ω). Note, that for the collisional broadening + dropping mass scenario (right panel) only the ρ and ω contributions as well as the sum of all sources are presented since the other individual contributions are similar to the bare mass case (left panel).

It is worth to point out, that already the free ρ -contribution is very asymmetric in mass due to the fact that the dilepton decay leads to a multiplication of the ρ -spectral function by $1/M^3$ (cf. Ref. [39]). This is in contrast to the assumption made in Ref. [46] for the e^+e^- spectra from $p+C$ and $p+Cu$ reactions at 12 GeV/ c laboratory momentum.

In order to see the differences between the results from the left and right panels of Fig. 2, a comparison of the different in-medium modification scenarios is shown in Fig. 3, *i.e.* collisional broadening (dashed lines) and collisional broadening + dropping vector meson masses (dash-dotted lines), with respect to the bare mass case (solid lines) on a

linear scale for $p + C$ from 1–4 GeV. At 1.0 GeV some enhancement for $0.4 \leq M \leq 0.5$ GeV in case of collisional broadening (dashed line) is found as well as an additional mass shift (dash-dotted line) which is essentially due to 'subthreshold' ρ production in the $\pi N \rightarrow N^*(1520) \rightarrow \rho N$ or $pN \rightarrow NN^*(1520) \rightarrow NN\rho$ reactions, where the ρ is stronger populated from the $N^*(1520)$ resonance in case of a broadened (and shifted) ρ spectral function. The modifications of the dilepton spectrum are rather moderate for the light C -target at 2, 3 and 4 GeV especially for the collisional broadening scenario since the ρ -nucleon-resonance couplings are already included dynamically in the transport model. Only in case of the additional ρ mass shift (dash-dotted lines) one observes a small enhancement for $0.5 \leq M \leq 0.75$ GeV, which is most pronounced at 3 GeV.

In Figs. 4–5 the calculational results for the $p + Ca$ reaction from 1–4 GeV are presented in analogy to Figs. 2 and 3. Consequently, the assignment of the individual lines is the same as in Figs. 2, 3 for the $p + C$ case. Except from an overall scaling in height, these spectra look very much the same as for the light C target. The in-medium modifications again can be much better seen by a direct comparison on a linear scale in Fig. 5. As mentioned before, collisional broadening of the ρ spectral function gives no net signal within the numerical statistics achieved whereas the 'dropping mass' scenario leads to a now more pronounced enhancement in the range $0.5 \leq M \leq 0.75$ GeV, which is up to a factor 1.7 at 3 GeV. Note, that this enhancement correlates with a reduction of the dilepton yield in the pole-mass region of the ρ and ω mesons.

Let's continue with the heavy Pb target. In Figs. 6–7 the calculated results for $p + Pb$ from 1–4 GeV are presented again in analogy to Figs. 2 and 3 with the same assignment of the individual lines. Apart from an overall scaling in height, these spectra look again very similar as for the C and Ca targets. The in-medium modifications again can be much better seen by a direct comparison on a linear scale in Fig. 7. Now the in-medium effects show up more clearly. Whereas collisional broadening of the ρ spectral function again gives no clear signal within the numerical accuracy achieved the 'dropping mass' scenario leads to a pronounced modification of the spectral shape. A strong reduction of the dilepton yield in the vector meson pole mass region around 0.77 GeV is observed since

most of the ρ 's and ω 's now decay in the medium approximately at density ρ_0 . This leads to a pronounced peak around $M \approx 0.65$ GeV, which can be attributed to the in-medium ω decay since the ρ spectral strength is distributed over a wide low mass regime. The situation is very reminiscent of dilepton spectra from $\pi + A$ and $\gamma + A$ reactions in Refs. [23,27,29]. Especially when comparing dilepton spectra from C and Pb targets, it should be experimentally possible to distinguish an in-medium mass shift of the ω meson by taking the ratio of both spectra.

In summarizing the results from Figs. 3, 5 and 7, the collisional broadening scenario gives practically the same dilepton spectra (within statistical fluctuations) as the bare mass case, since the coupling of the ρ 's to the baryonic resonances are dynamically taken into account in the resonance model. The inclusion of 'dropping' vector meson masses leads to an enhancement of the dilepton yield for $M = 0.5 - 0.75$ GeV and to a reduction at the ω -peak which becomes more pronounced with increasing target size and indicates a factor of 2 enhancement from in-medium ω decays in case of $p + Pb$ at 3–4 GeV.

2. Transverse momentum distributions

In Fig. 8 the transverse momentum distribution of all dileptons for the $p + C$ system at 1.0 , 2.0, 3.0 and 4.0 GeV are displayed. Here the sequence of the individual channels is as follows: the contribution from the π^0 Dalitz decay dominates at all energies and is practically identical to the sum of all sources (solid line). Apart from 1.0 GeV the next strong channel is the η Dalitz decay followed by the Δ -Dalitz decays, pn bremsstrahlung and the ω -Dalitz decays, while the direct decays of the ρ and ω mesons are down by orders of magnitude. Thus global p_T spectra do not provide very interesting information.

In order to extract the interesting physics one has to apply cuts on the invariant dilepton mass to suppress or exclude the dominant channels. For this purpose a cut on the interval $0.4 \leq M \leq 0.7$ GeV has been chosen, which is displayed for the $p + C$ reaction at 2.0, 3.0 and 4.0 GeV in Fig. 9 (left panel) for the bare mass case. Indeed, now the ρ meson signal is the strongest or at least comparable to the remaining η Dalitz

decay, whereas the other channels are more suppressed. In the right panel of Fig. 9 a comparison of the bare mass case (solid lines) with the collisional broadening and dropping mass scenario (dash-dotted lines) is presented. Since the differences are only very tiny, one can conclude that there is practically no sensitivity to in-medium effects for the C target at all energies.

Following the same strategy as in the previous subsection the same analysis for the system $p + Ca$ is shown in Figs. 10 and 11. The p_T spectrum of the dileptons is again similar at all energies to that from the C target in Figs. 8 and 9, however, the detailed comparison of the bare mass (solid line) and dropping mass + collisional broadening scenario (dash-dotted line) in Fig. 11 (right panel) indicates an enhancement of the p_T spectrum in case of the in-medium modifications whereas the shape in p_T is very similar. These observations are practically identical even for the heavy Pb target as demonstrated in Figs. 12 and 13. Here the p_T spectrum from the different scenarios (right panel in Fig. 13) show the same enhancement for the dropping mass case as in Fig. 11, however, the spectral shape in p_T does not provide new information since it does not differ significantly at any transverse momentum.

3. Dilepton rapidity distributions

In Fig. 14 the rapidity distribution of all dileptons in the laboratory for the $p + C$ system at 1.0 , 2.0, 3.0 and 4.0 GeV is displayed. Here the sequence of the individual lines is follows: the contribution from the π^0 Dalitz decay dominates at all energies and again is almost identical to the sum of all sources (solid line). Apart from 1.0 GeV the next strong channel is the η Dalitz decay followed by the Δ -Dalitz decays, pn bremsstrahlung and the ω -Dalitz decays, while the direct decays of the ρ and ω mesons are again barely visible.

In order to extract the interesting information cuts on the invariant dilepton mass are necessary to suppress/exclude the dominant channels. Again a cut on the interval $0.4 \leq M \leq 0.7$ GeV has been chosen, which is displayed for the $p + C$ reaction at 2.0,

3.0 and 4.0 GeV in Fig. 15 (left panel) for the bare mass case. Indeed, now the ρ meson signal is the strongest or comparable to the remaining η Dalitz decay (which will be even more suppressed by gating on the interval $0.55 \leq M \leq 0.75$ GeV). In the right panel of Fig. 15 a comparison of the bare mass case (solid lines) with the collisional broadening and dropping mass scenario (dash-dotted lines) is presented. As in case of the p_T spectra the differences are only very tiny; one thus can conclude that there is no sensitivity to in-medium effects for the C target with respect to rapidity spectra, too.

For completeness, in Figs. 16 to 19 the same analysis is shown for the Ca and Pb target at all energies. As seen from the right panels in Figs. 17 and 19 the shape of the rapidity distribution is not changed very much for the in-medium mass scenario compared to the bare mass case except for a tiny shift to lower laboratory rapidities. As in case of the p_T spectra in the previous subsection, an overall enhancement in the dilepton yield for the in-medium mass scenario for the $p + Pb$ reaction is the most pronounced effect.

4. Double differential dilepton spectra

Finally, in Fig. 20 the double differential dilepton spectrum $d\sigma/dMdp_T$ is presented as a function of the invariant mass M and transverse momentum p_T for $p + Pb$ collisions at 4.0 GeV calculated within the bare mass scenario. At fixed p_T one can recognize the shape of the invariant mass spectra (cf. left panel of Fig. 6) with a strong π^0 Dalitz decay branch at low M as well as the contributions from η Dalitz decay and the vector meson (ρ, ω) decays. At fixed M the shape looks similar to the one in Fig. 6. At low M the exponential decrease stems from the π^0 Dalitz decay, then the spectra become flatter due to the contributions from η Dalitz ($M \leq 0.4$ GeV) and direct ρ decays. At $M \sim 0.78$ GeV the peak from the direct decay of ω mesons is visible. Thus, such type of 3-dimensional experimental information (or even 4-dimensional including rapidity) allows to select the contributions from different channels.

V. SUMMARY

Within the framework of the coupled-channel (resonance) BUU model a detailed non-perturbative study of dilepton production for $p + A$ reactions from 1–4 GeV has been performed employing a full off-shell propagation of the vector mesons in line with Refs. [42,43]. Different scenarios of in-medium modifications of vector mesons, such as collisional broadening and dropping vector meson masses, have been investigated and the possibilities for an experimental observation of in-medium effects in $p + A$ reactions has been discussed.

Dilepton spectra from $p + A$ reactions will be measured in future by the HADES Collaboration at GSI Darmstadt with high mass resolution and good accuracy. In this respect predictions for the dilepton invariant mass spectra, transverse momentum and rapidity distributions for $p + C$, $p + Ca$ and $p + Pb$ collisions from 1 to 4 GeV have been made employing different in-medium scenarios. It has been found that the collisional broadening + 'dropping mass' scenario leads to an enhancement of the dilepton yield in the range $0.5 \leq M \leq 0.75$ GeV and to a reduction of the ω -peak, which is more pronounced for heavy systems (up to a factor 2 for $p + Pb$ at 3–4 GeV).

It has been indicated that proper cuts in invariant mass for transverse momentum and rapidity spectra allow to select different dilepton sources and to study, for example, the ρ meson channel in more detail. However, an inclusion of in-medium effects predominantly leads to an overall scaling in height of the spectra, but does not change the slope of the p_T and rapidity distributions very much.

It has been indicated, furthermore, that it might be very useful to provide experimentally multi-dimensional information, e.g. double differential dilepton spectra $d\sigma/dMdp_T$, in order to investigate the individual contributions.

ACKNOWLEDGMENTS

The author is grateful to U. Mosel, who initiated this work, for useful suggestions and to W. Cassing for valuable discussions on the question of off-shell transport theory.

REFERENCES

- [1] G.E. Brown and M. Rho, Phys. Rev. Lett. 66 (1991) 2720.
- [2] C.M. Shakin and W.-D. Sun, Phys. Rev. C 49 (1994) 1185.
- [3] F. Klingl and W. Weise, Nucl. Phys. A 606 (1996) 329; F. Klingl, N. Kaiser and W. Weise, Nucl. Phys. A 624 (1997) 527.
- [4] T. Hatsuda and S. Lee, Phys. Rev. C 46 (1992) R34.
- [5] M. Asakawa and C.M. Ko, Phys. Rev. C 48 (1993) R526.
- [6] S. Leupold, W. Peters and U. Mosel, Nucl. Phys. A 628 (1998) 311.
- [7] M. Herrmann, B. Friman, and W. Nörenberg, Nucl. Phys. A 560 (1993) 411.
- [8] M. Asakawa, C. M. Ko, P. Lévai, and X. J. Qiu, Phys. Rev. C 46 (1992) R1159.
- [9] G. Chanfray and P. Schuck, Nucl. Phys. A 545 (1992) 271c.
- [10] R. Rapp, G. Chanfray, and J. Wambach, Phys. Rev. Lett. 76 (1996) 368.
- [11] B. Friman and H. J. Pirner, Nucl. Phys. A 617 (1997) 496.
- [12] R. Rapp, G. Chanfray and J. Wambach, Nucl. Phys. A 617 (1997) 472.
- [13] W. Peters, M. Post, H. Lenske, S. Leupold, and U. Mosel, Nucl. Phys. A 632 (1998) 109; M. Post, S. Leupold and U. Mosel, nucl-th/0008027.
- [14] G. Agakichiev et al., Phys. Rev. Lett. 75 (1995) 1272.
- [15] Th. Ullrich et al., Nucl. Phys. A 610 (1996) 317c; A. Drees, Nucl. Phys. A 610 (1996) 536c.
- [16] M. A. Mazzoni, Nucl. Phys. A 566 (1994) 95c; M. Maserà, Nucl. Phys. A 590 (1995) 93c.
- [17] T. Åkesson et al., Z. Phys. C 68 (1995) 47.
- [18] G. Q. Li, C. M. Ko, and G. E. Brown, Phys. Rev. Lett. 75 (1995) 4007.

- [19] C. M. Ko, G. Q. Li, G. E. Brown, and H. Sorge, Nucl. Phys. A 610 (1996) 342c.
- [20] W. Cassing, W. Ehehalt, and C. M. Ko, Phys. Lett. B 363 (1995) 35.
- [21] W. Cassing, W. Ehehalt, and I. Kralik, Phys. Lett. B 377 (1996) 5.
- [22] E. L. Bratkovskaya and W. Cassing, Nucl. Phys. A 619 (1997) 413.
- [23] W. Cassing and E. L. Bratkovskaya, Phys. Rep. 308 (1999) 65.
- [24] C. Ernst, S. A. Bass, M. Belkacem, H. Stöcker, and W. Greiner, Phys. Rev. C 58 (1998) 447.
- [25] M. Asakawa and C. M. Ko, Nucl. Phys. A 560 (1993) 399.
- [26] G. Q. Li, C. M. Ko, and G. E. Brown, Nucl. Phys. A 606 (1996) 568.
- [27] M. Effenberger, E. L. Bratkovskaya, W. Cassing and U. Mosel, Phys. Rev. C 60 (1999) 027601.
- [28] W. Cassing, E. L. Bratkovskaya, R. Rapp, and J. Wambach, Phys. Rev. C 57 (1998) 916.
- [29] M. Effenberger, E. Bratkovskaya and U. Mosel, Phys. Rev. C 60 (1999) 044614.
- [30] Gy. Wolf, G. Batko, W. Cassing, U. Mosel, K. Niita, and M. Schäfer, Nucl. Phys. A 517 (1990) 615; Gy. Wolf, W. Cassing and U. Mosel, Nucl. Phys. A 552 (1993) 549.
- [31] E. L. Bratkovskaya, W. Cassing and U. Mosel, Phys. Lett. B 376 (1996) 12.
- [32] M. Effenberger, Ph.D. Thesis, Univ. of Giessen, 1999; <http://theorie.physik.uni-giessen.de/ftp.html>.
- [33] K. G. Boreskov, J. Koch, L. A. Kondratyuk, and M. I. Krivoruchenko, Phys. of Atomic Nuclei 59 (1996) 1908; K. G. Boreskov, L. A. Kondratyuk, M. I. Krivoruchenko, and J. Koch, Nucl. Phys. A 619 (1997) 295.
- [34] S. Teis, W. Cassing, M. Effenberger, A. Hombach, U. Mosel, and Gy. Wolf, Z. Phys. A 356 (1997) 421; Z. Phys. A 359 (1997) 297.

- [35] D. M. Manley and E. M. Saleski, Phys. Rev. D 45 (1992) 4002.
- [36] B. Anderson, G. Gustafson and Hong Pi, Z. Phys. C 57 (1993) 485.
- [37] W. Ehehalt and W. Cassing, Nucl. Phys. A 602 (1996) 449.
- [38] S. A. Bass et al., Prog. Part. Nucl. Phys. 42 (1998) 279; J. Phys. G 25 (1999) 1859.
- [39] E.L. Bratkovskaya, W. Cassing and U. Mosel, Nucl. Phys. A 686 (2001) 476.
- [40] A. Faessler, C. Fuchs and M.I. Krivoruchenko, Phys. Rev. C 61 (2000) 035206.
- [41] W. Cassing, Ye. S. Golubeva, A. S. Iljinov, and L. A. Kondratyuk, Phys. Lett. B 396 (1997) 26; Ye. S. Golubeva, L. A. Kondratyuk and W. Cassing, Nucl. Phys. A 625 (1997) 832.
- [42] W. Cassing and S. Juchem, Nucl. Phys. A 665 (2000) 377.
- [43] W. Cassing and S. Juchem, Nucl. Phys. A 672 (2000) 417.
- [44] S. Leupold, Nucl. Phys. A 672 (2000) 475.
- [45] L. A. Kondratyuk, A. Sibirtsev, W. Cassing, Ye. S. Golubeva, and M. Effenberger, Phys. Rev. C 58 (1998) 1078.
- [46] K. Ozawa et al., nucl-ex/0011013.

FIGURES

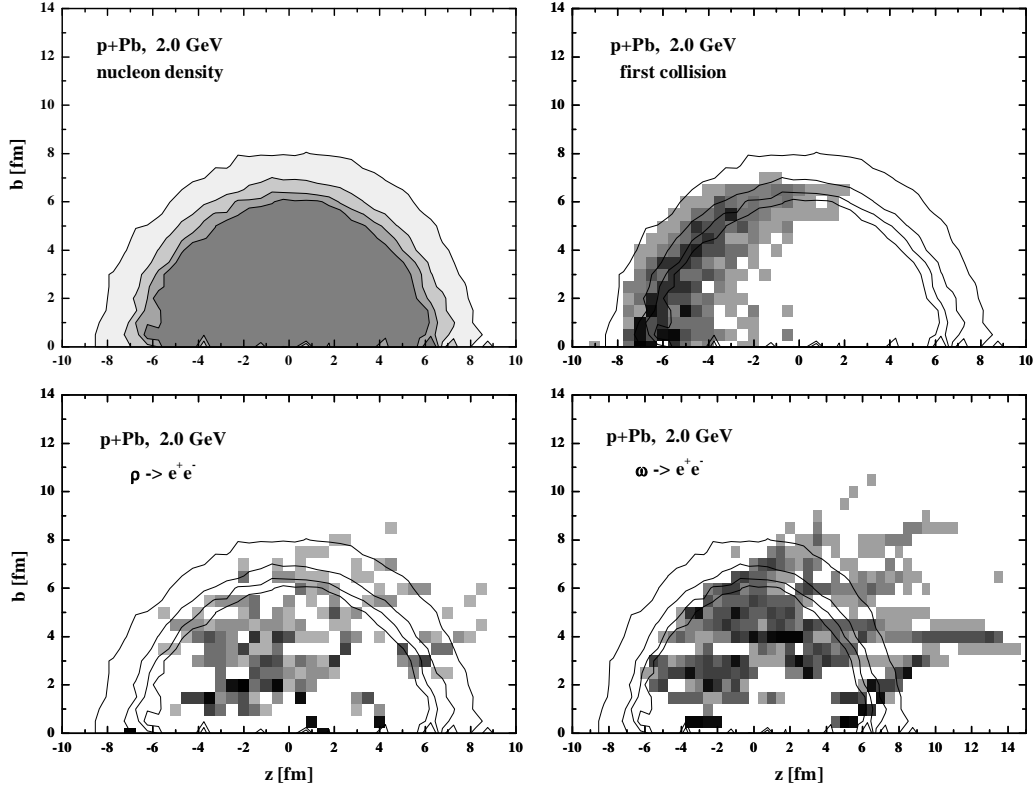


FIG. 1. Upper left part – the average density distribution of a Pb -nucleus at rest in the laboratory; upper right part – the spatial distribution in the first pN collisions; lower part – the spatial distribution for ρ -meson (left part) and ω -meson (right part) decays to dileptons. The contour lines correspond to densities of $0.1\rho_0$, $0.4\rho_0$, $0.6\rho_0$ and $0.8\rho_0$ respectively, and the dark shaded area to $\rho \geq 0.8\rho_0$.

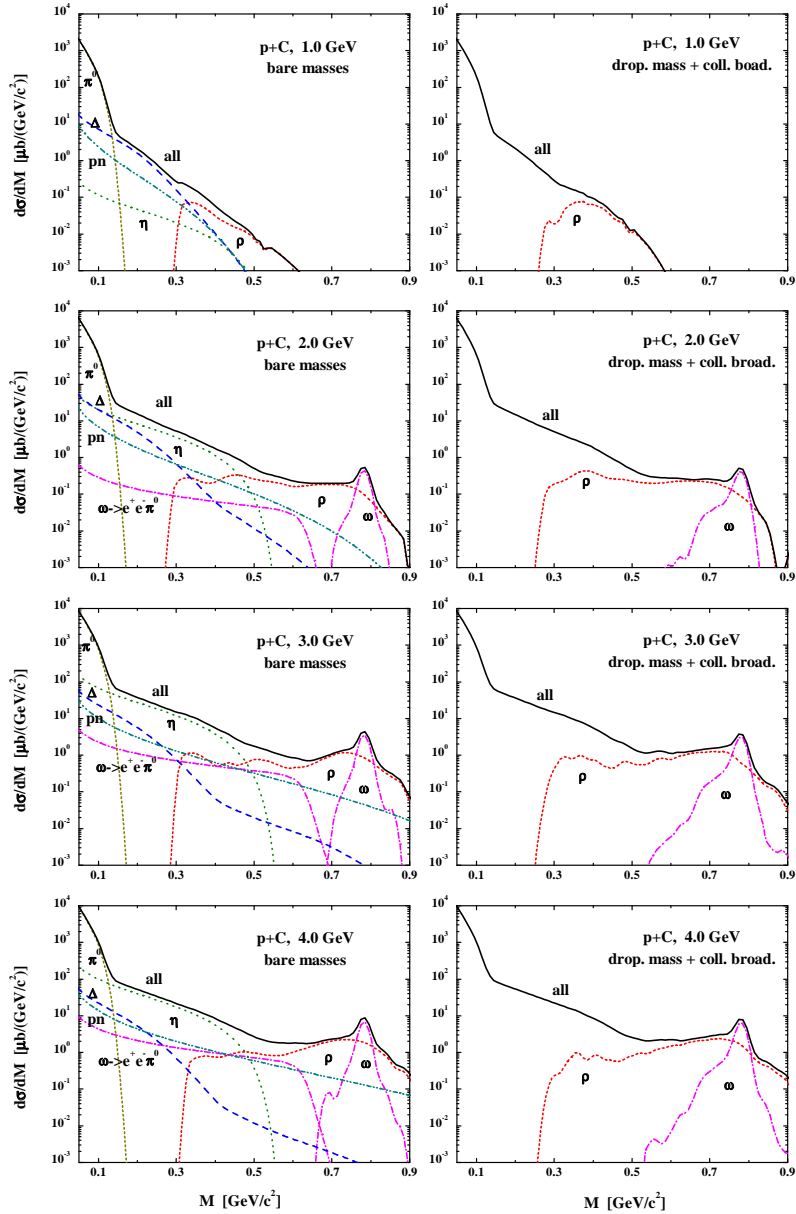


FIG. 2. The calculated dilepton invariant mass spectra $d\sigma/dM$ for $p+C$ collisions from 1 – 4 GeV (including an experimental mass resolution of 10 MeV) without in-medium modifications (bare masses) – left part, and applying the collisional broadening + dropping mass scenario – right part. The thin lines indicate the individual contributions from the different production channels; *i.e.* starting from low M : Dalitz decay $\pi^0 \rightarrow \gamma e^+e^-$ (short dashed line), $\eta \rightarrow \gamma e^+e^-$ (dotted line), $\Delta \rightarrow N e^+e^-$ (dashed line), $\omega \rightarrow \pi^0 e^+e^-$ (dot-dashed line), for $M \approx 0.7$ GeV: $\omega \rightarrow e^+e^-$ (dot-dashed line), $\rho^0 \rightarrow e^+e^-$ (short dashed line). The full solid line represents the sum of all sources considered here.

e

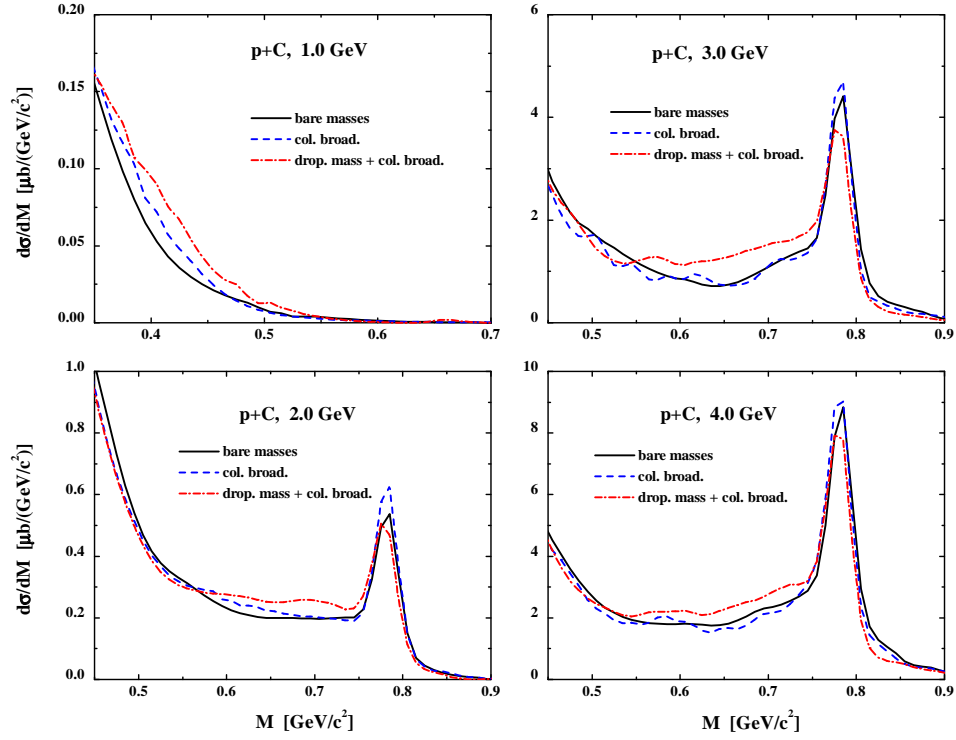


FIG. 3. The comparison of different in-medium modification scenarios, i.e. collisional broadening (dashed lines) and collisional broadening + dropping vector meson masses (dash-dotted lines), with respect to the bare mass case (solid lines) on a linear scale for $p + C$ from 1–4 GeV.

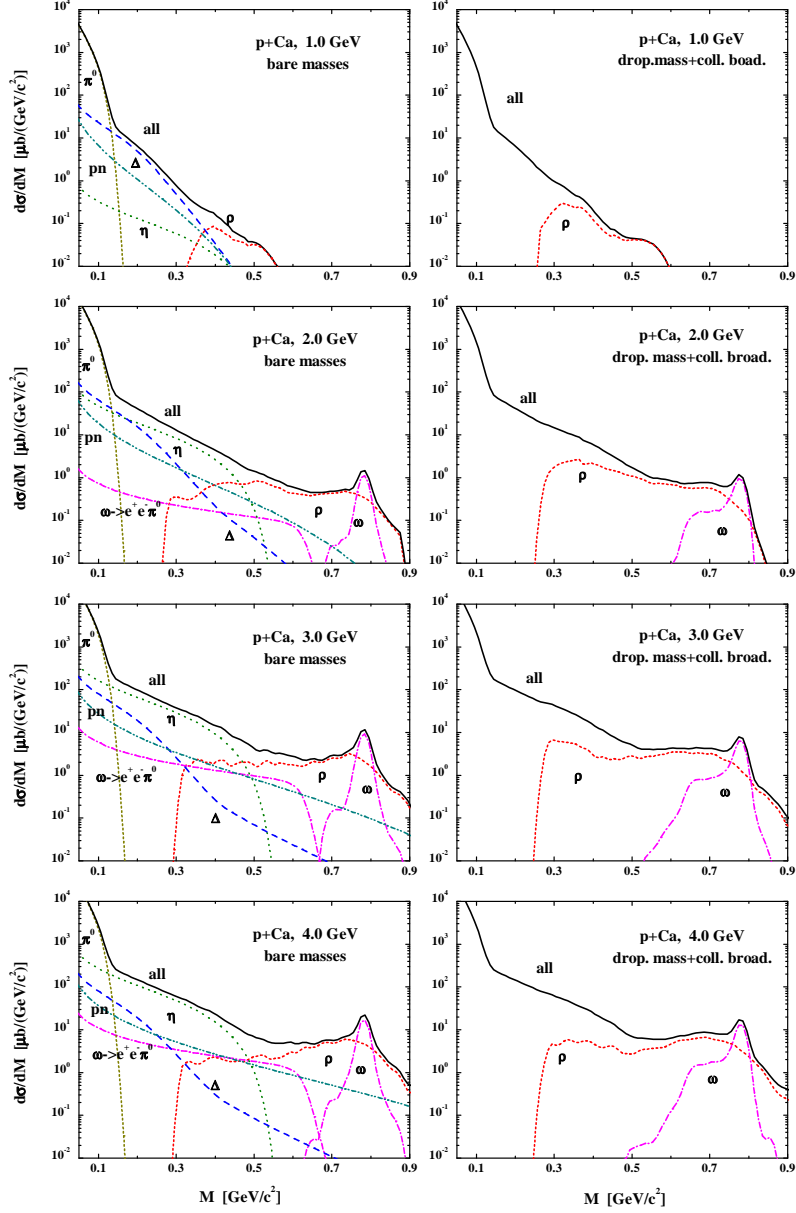


FIG. 4. The calculated dilepton invariant mass spectra $d\sigma/dM$ for $p+Ca$ collisions from 1.0 – 4 GeV (including an experimental mass resolution of 10 MeV) without in-medium modifications (bare masses) – left part, and applying the collisional broadening + dropping masses scenario – right part. The assignment of the individual lines is the same as in Fig. 2.

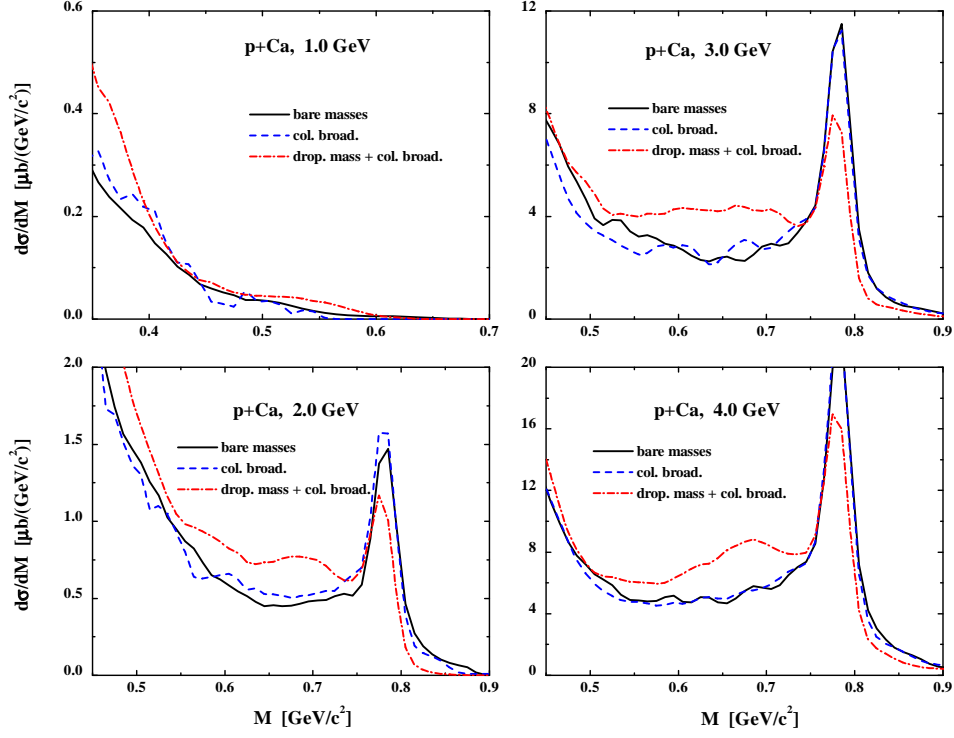


FIG. 5. The comparison of different in-medium modification scenarios, i.e. collisional broadening (dashed lines) and collisional broadening + dropping vector meson masses (dash-dotted lines), with respect to the bare mass case (solid lines) on a linear scale for $p+Ca$ from 1–4 GeV.

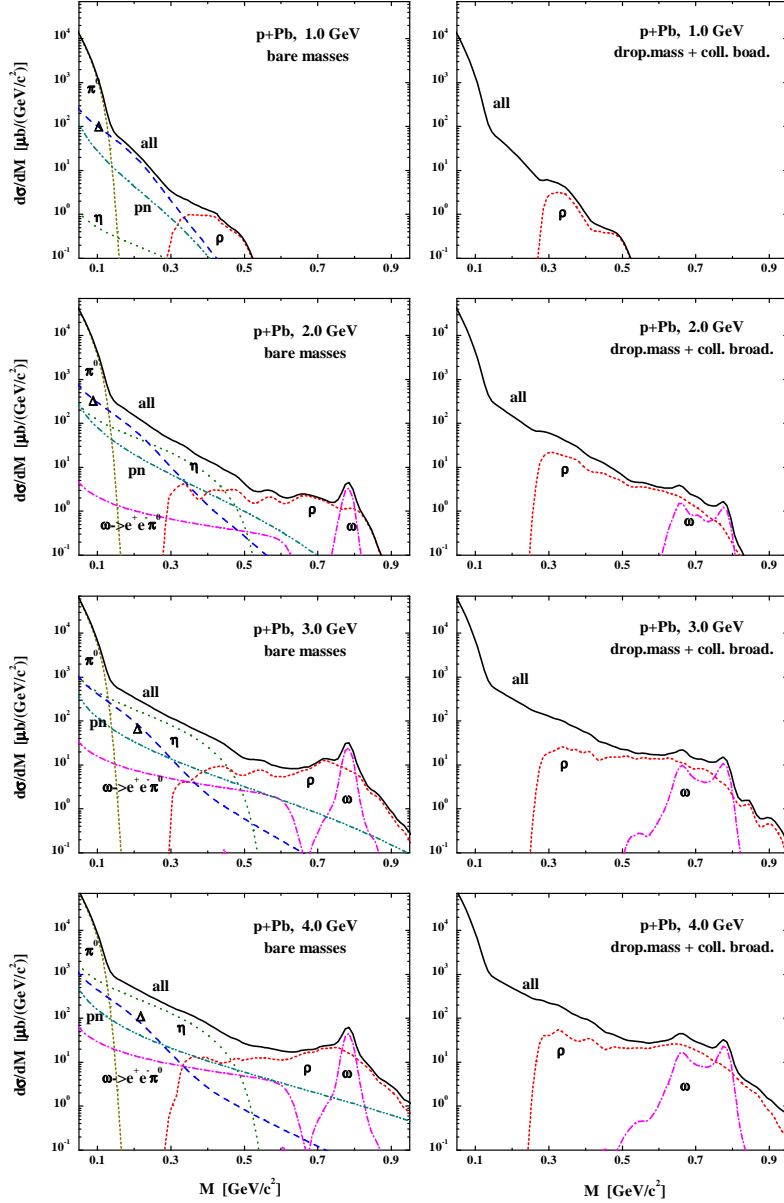


FIG. 6. The calculated dilepton invariant mass spectra $d\sigma/dM$ for $p+Pb$ collisions from 1.0 – 4 GeV (including an experimental mass resolution of 10 MeV) without in-medium modifications (bare masses) – left part, and applying the collisional broadening + dropping masses scenario – right part. The assignment of the individual lines is the same as in Fig. 2.

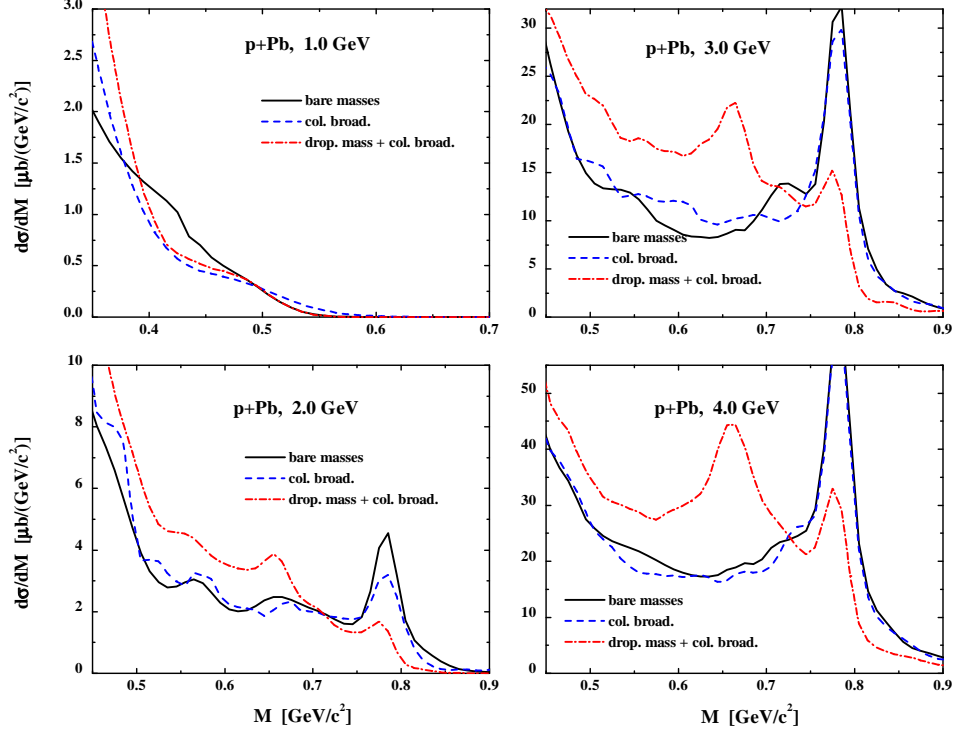


FIG. 7. The comparison of different in-medium modification scenarios, i.e. collisional broadening (dashed lines) and collisional broadening + dropping vector meson masses (dash-dotted lines), with respect to the bare mass case (solid lines) on a linear scale for $p + Pb$ from 1–4 GeV.

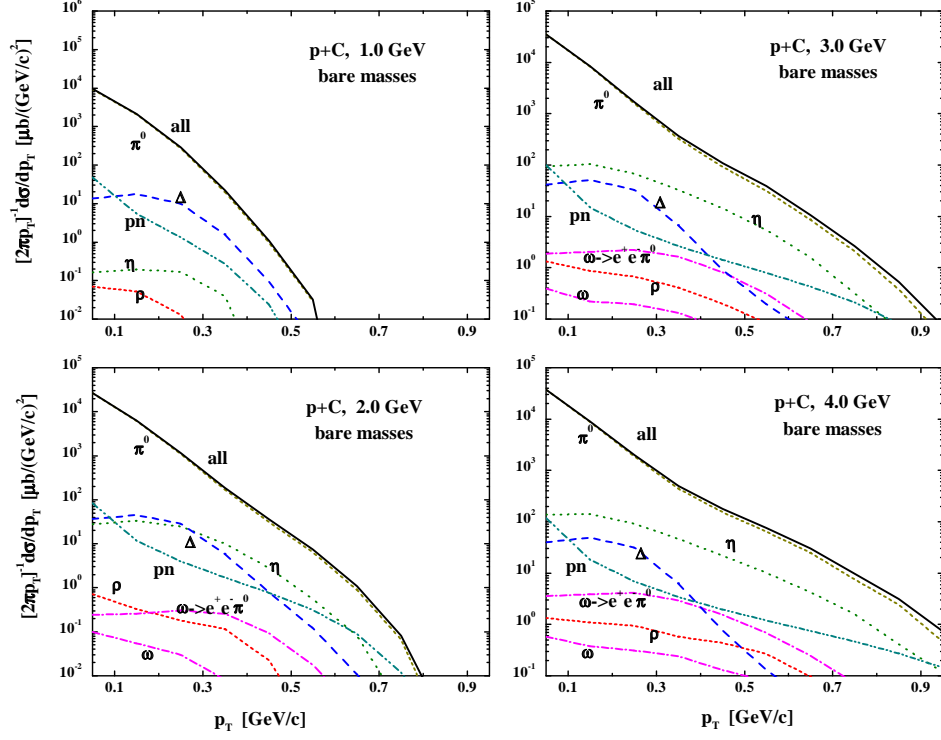


FIG. 8. The transverse momentum distribution $d\sigma/dp_T/(2\pi p_T)$ for the $p + C$ system at 1.0, 2.0, 3.0 and 4.0 GeV.

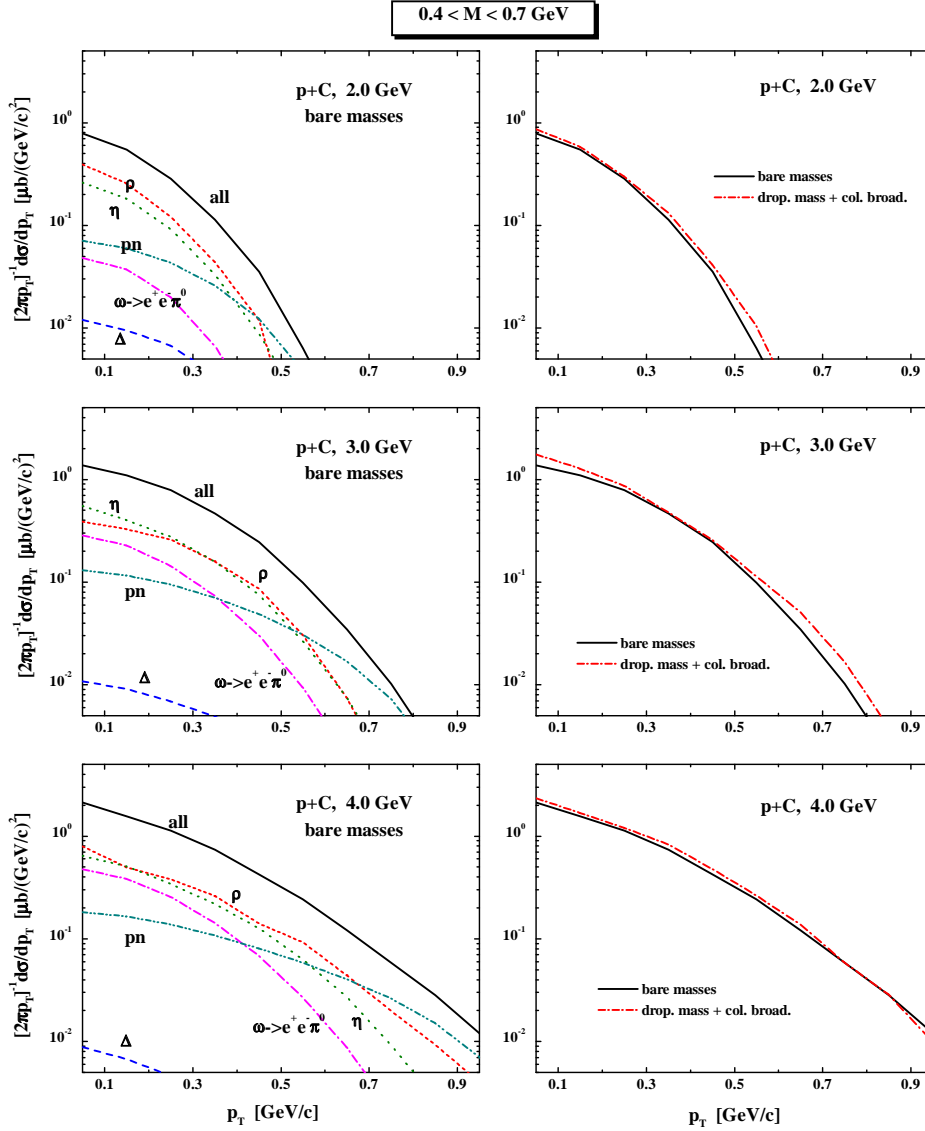


FIG. 9. The transverse momentum distribution $d\sigma/dp_T/(2\pi p_T)$ for the $p+C$ system at 1.0, 2.0, 3.0 and 4.0 GeV implying a cut in invariant mass of $0.4 \leq M \leq 0.7$ GeV. Left panel – the individual contributions for bare mass case, right panel - comparison of the bare mass spectra (solid line) with the collisional broadening and dropping mass scenario (dash-dotted lines).

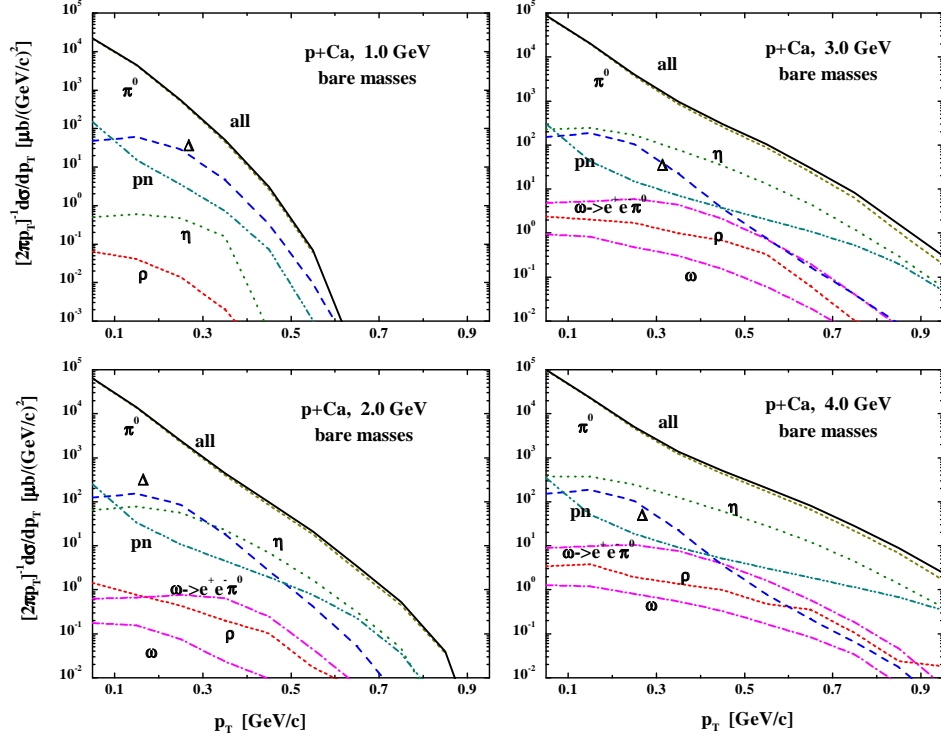


FIG. 10. The transverse momentum distribution $d\sigma/dp_T/(2\pi p_T)$ for the $p + Ca$ system at 1.0, 2.0, 3.0 and 4.0 GeV.

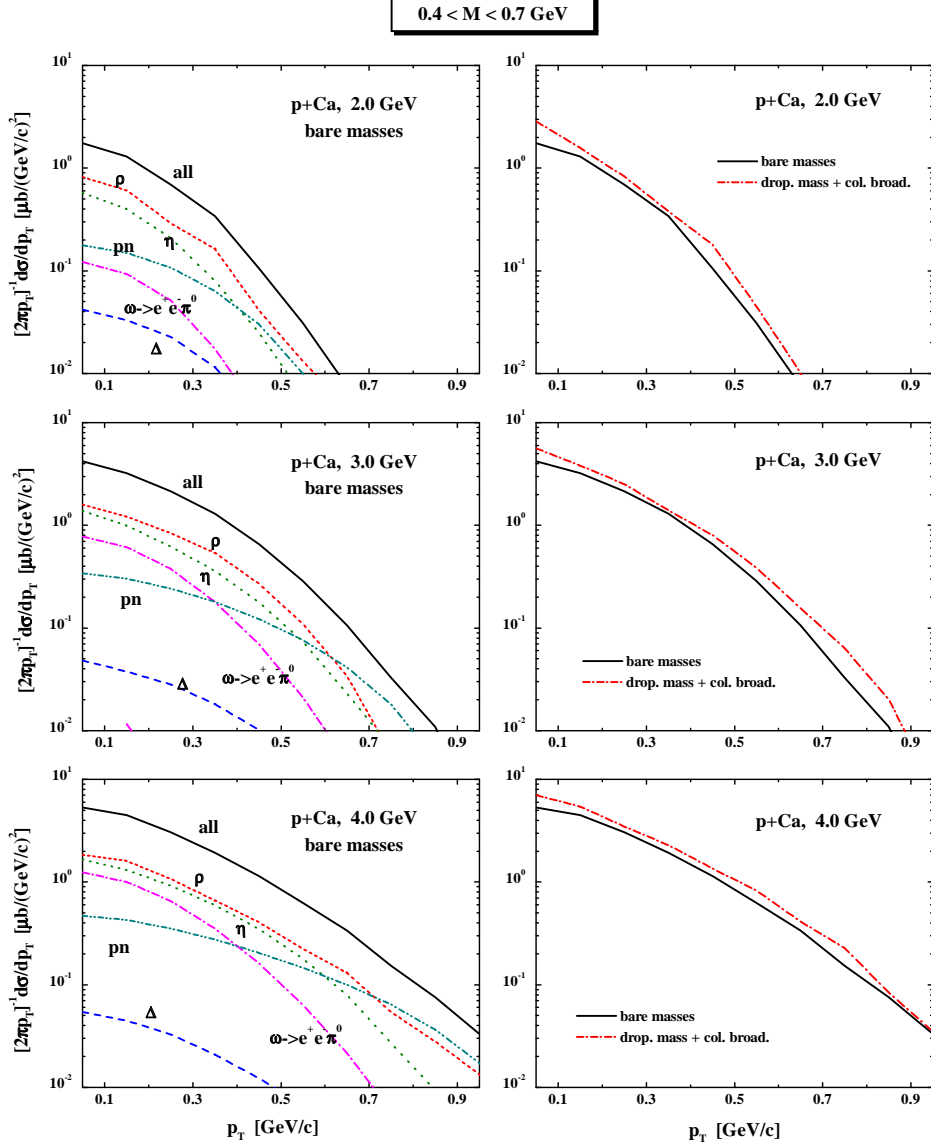


FIG. 11. The transverse momentum distribution $d\sigma/dp_T/(2\pi p_T)$ for the $p + Ca$ system at 1.0, 2.0, 3.0 and 4.0 GeV implying a cut in invariant mass of $0.4 \leq M \leq 0.7$ GeV. Left panel – the individual contributions for bare mass case, right panel - comparison of the bare mass spectra (solid line) with the collisional broadening and dropping mass scenario (dash-dotted lines).

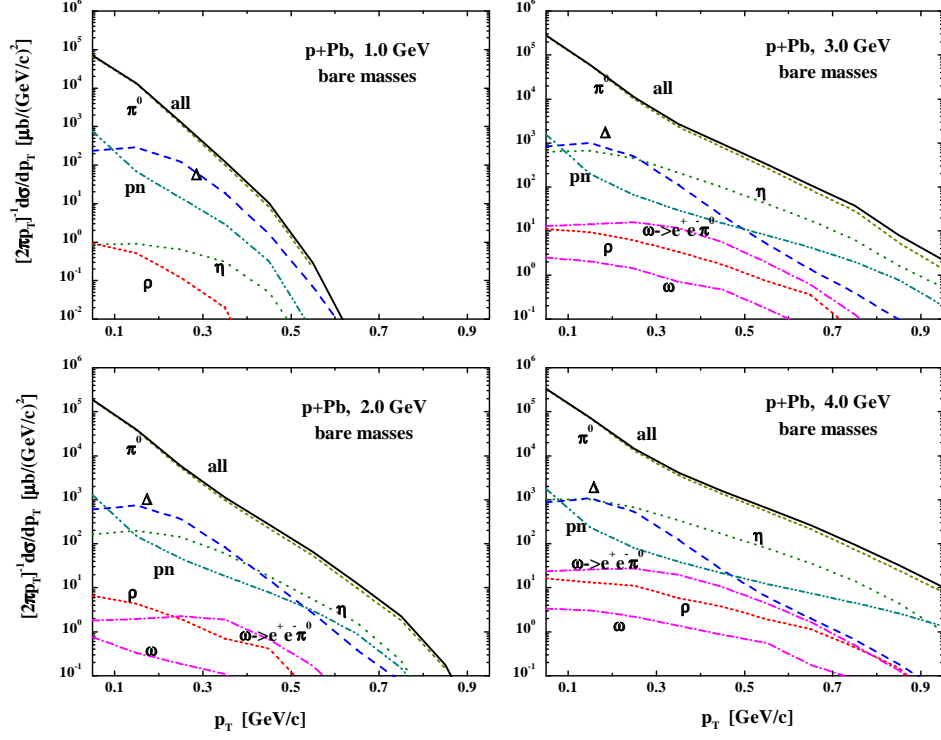


FIG. 12. The transverse momentum distribution $d\sigma/dp_T/(2\pi p_T)$ for the $p + Pb$ system at 1.0, 2.0, 3.0 and 4.0 GeV.

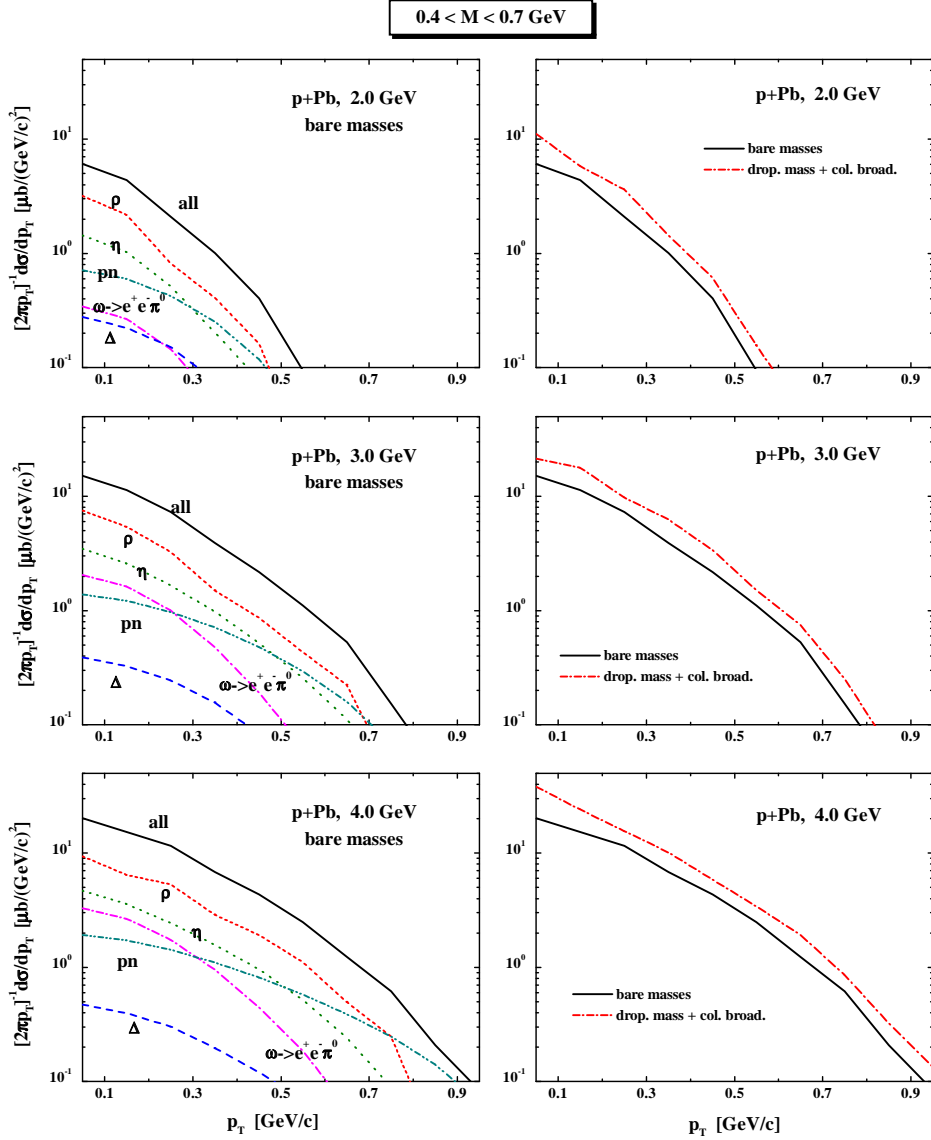


FIG. 13. The transverse momentum distribution $d\sigma/dp_T/(2\pi p_T)$ for the $p + Pb$ system at 1.0, 2.0, 3.0 and 4.0 GeV implying a cut in invariant mass of $0.4 \leq M \leq 0.7$ GeV. Left panel – the individual contributions for bare mass case, right panel - comparison of the bare mass spectra (solid line) with the collisional broadening and dropping mass scenario (dash-dotted lines).

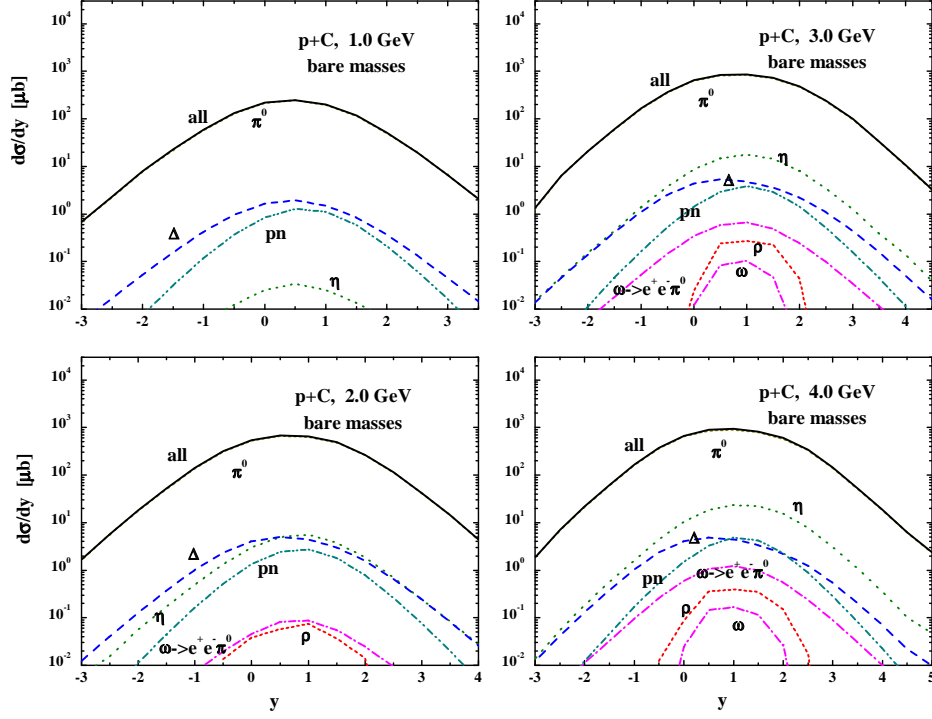


FIG. 14. The laboratory rapidity distributions $d\sigma/dy$ for the $p + C$ system at 1.0, 2.0, 3.0 and 4.0 GeV.

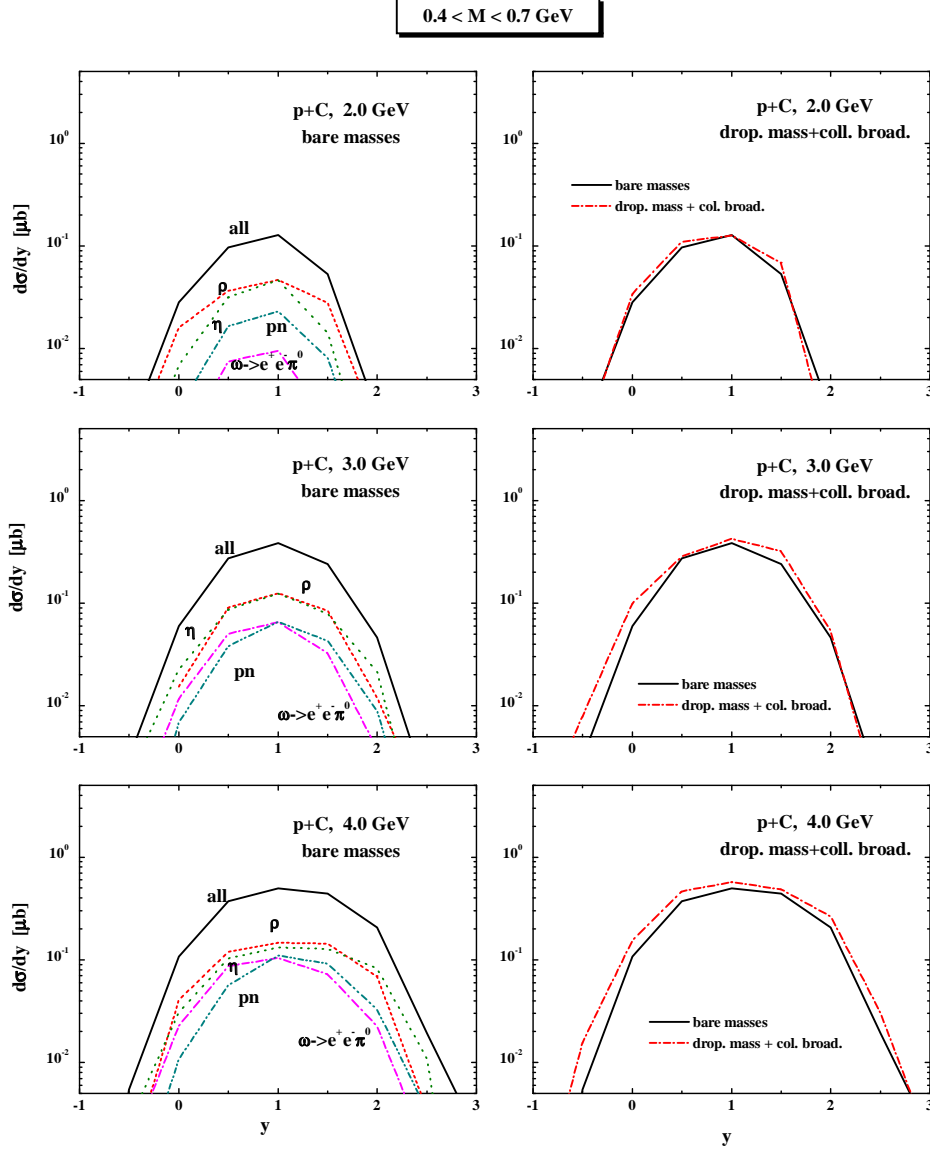


FIG. 15. The laboratory rapidity distributions $d\sigma/dy$ for $p + C$ system at 1.0, 2.0, 3.0 and 4.0 GeV implying a cut in invariant mass of $0.4 \leq M \leq 0.7$ GeV. Left panel – the individual contributions for bare mass case, right panel - comparison of the bare mass spectra (solid line) with the collisional broadening and dropping mass scenario (dash-dotted lines).

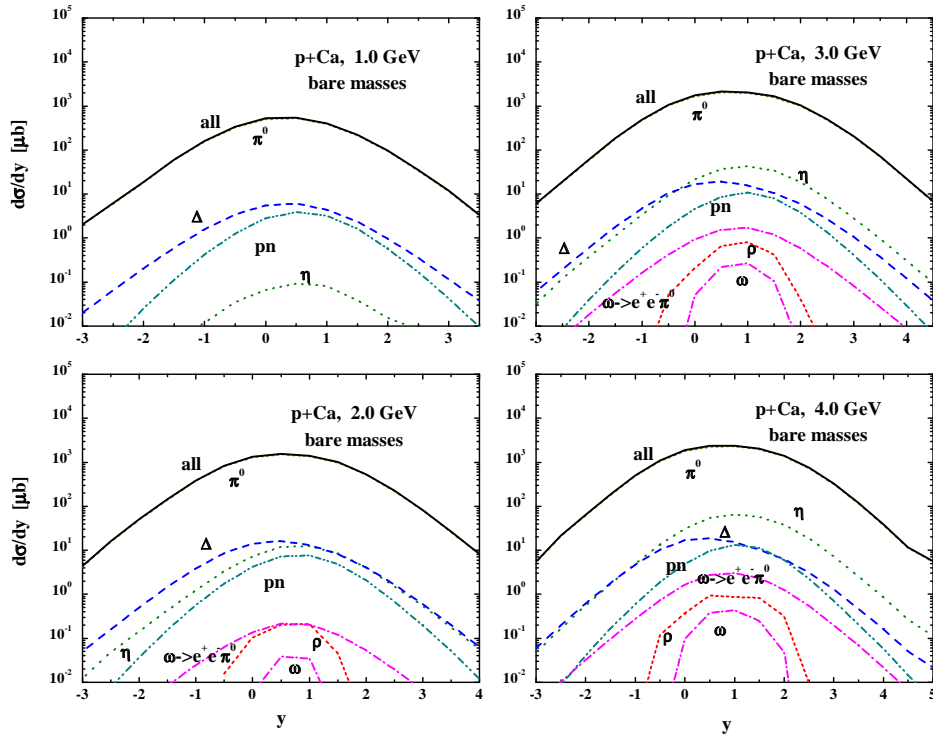


FIG. 16. The laboratory rapidity distributions $d\sigma/dy$ for the $p+Ca$ system at 1.0, 2.0, 3.0 and 4.0 GeV.

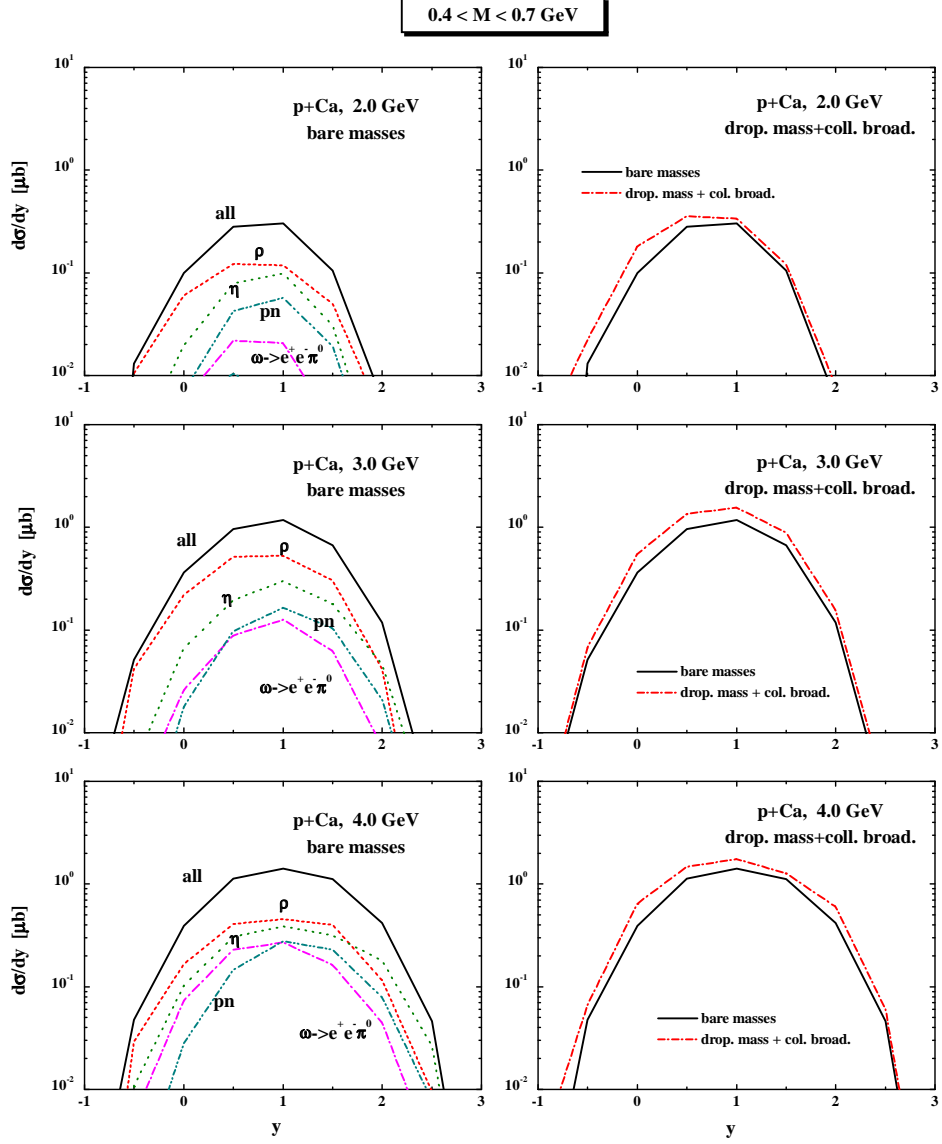


FIG. 17. The laboratory rapidity distributions $d\sigma/dy$ for $p + Ca$ system at 1.0, 2.0, 3.0 and 4.0 GeV implying a cut in invariant mass of $0.4 \leq M \leq 0.7 \text{ GeV}$. Left panel – the individual contributions for bare mass case, right panel - comparison of the bare mass spectra (solid line) with the collisional broadening and dropping mass scenario (dash-dotted lines).

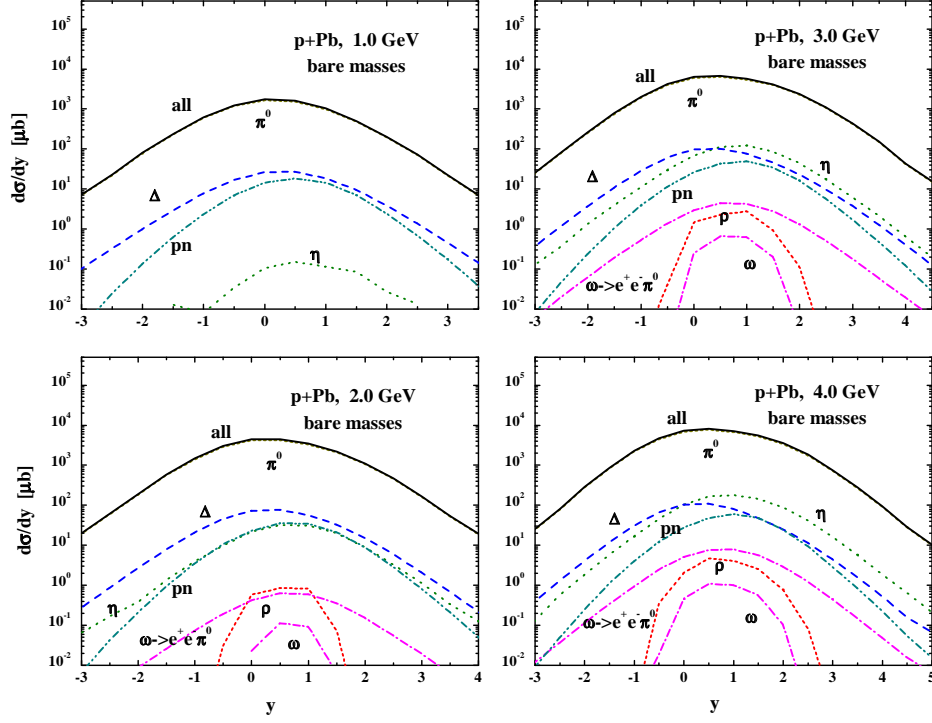


FIG. 18. The laboratory rapidity distributions $d\sigma/dy$ for the $p + Pb$ system at 1.0, 2.0, 3.0 and 4.0 GeV.

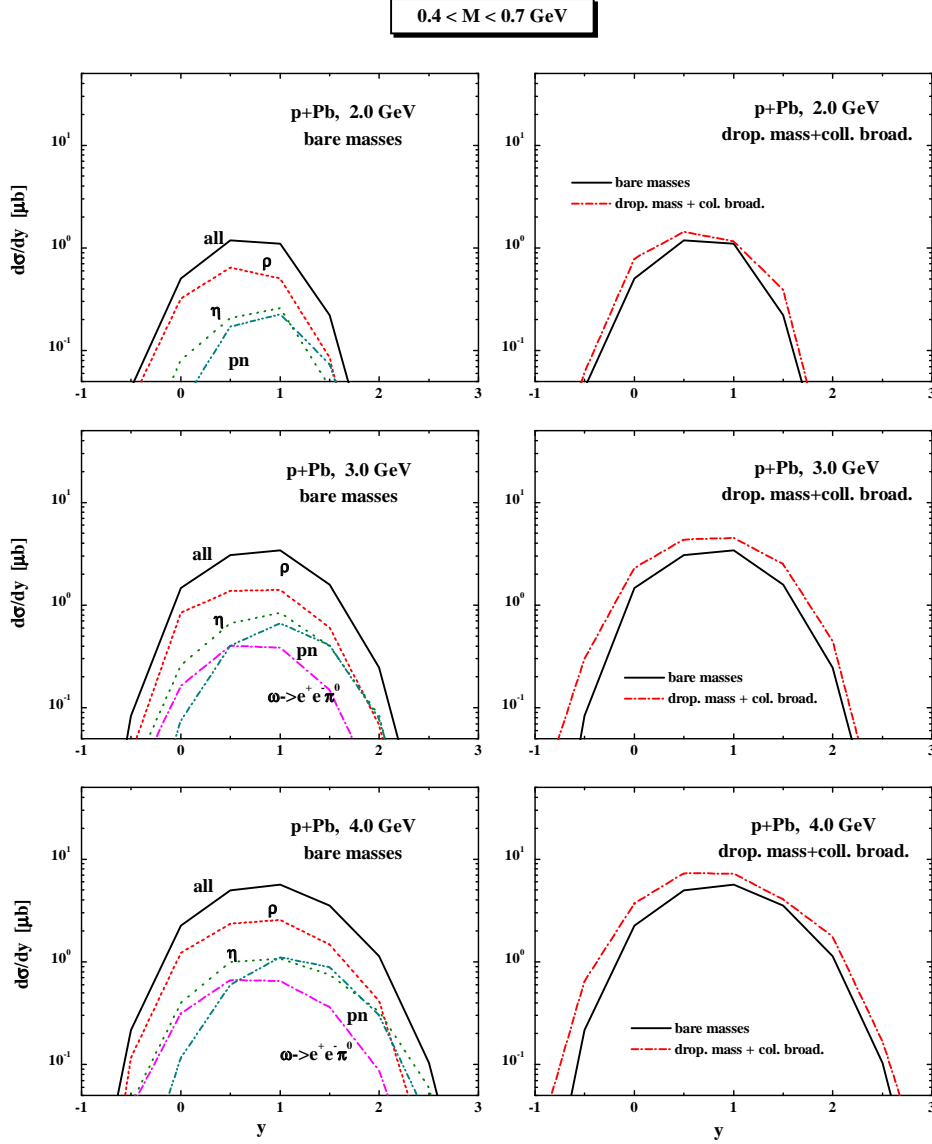


FIG. 19. The laboratory rapidity distributions $d\sigma/dy$ for $p+Pb$ system at 1.0, 2.0, 3.0 and 4.0 GeV implying a cut in invariant mass of $0.4 \leq M \leq 0.7 \text{ GeV}$. Left panel – the individual contributions for bare mass case, right panel - comparison of the bare mass spectra (solid line) with the collisional broadening and dropping mass scenario (dash-dotted lines).

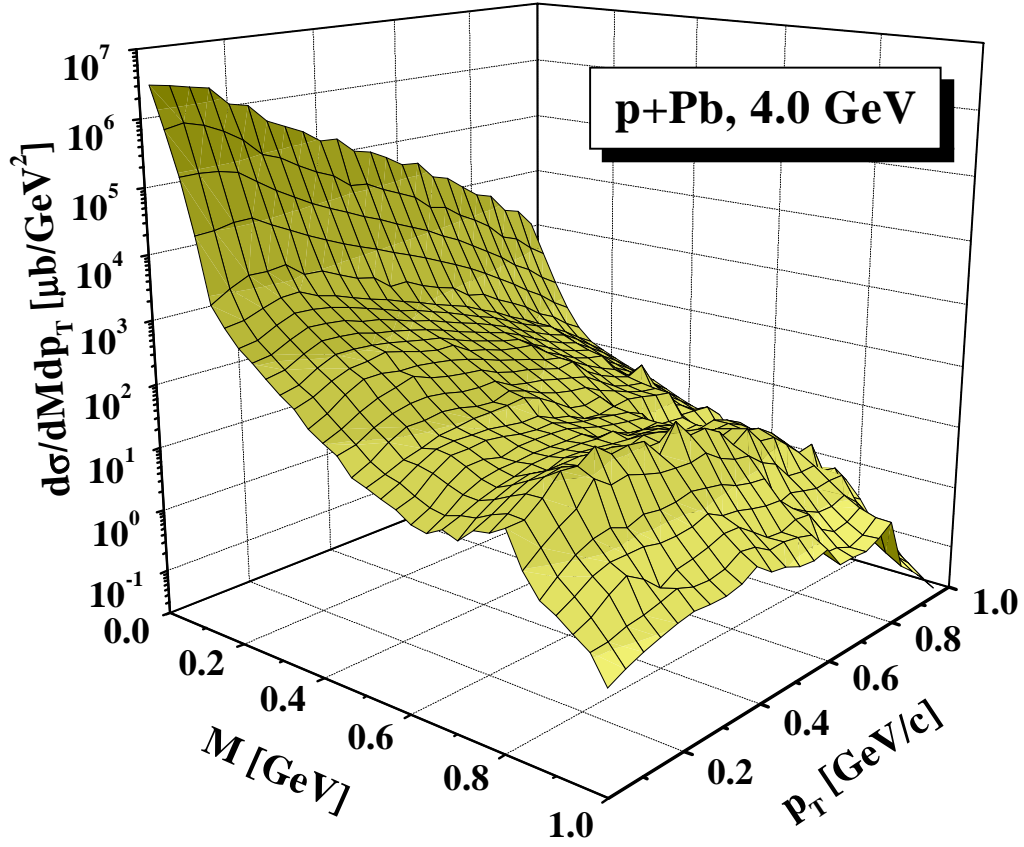


FIG. 20. The calculated double differential dilepton spectra $d\sigma/dMdp_T$ as a function of invariant mass M and transverse momentum p_T for $p + Pb$ collisions at 4.0 GeV.